ACS APPLIED MATERIALS & INTERFACES

Research Article

Cite This: ACS Appl. Mater. Interfaces 2018, 10, 38280−38286

www.acsami.org

Improved Room Temperature NO_2 Sensing Performance of Organic Field-Effect Transistor by Directly Blending a Hole-Transporting/Electron-Blocking Polymer into the Active Layer

Shijiao Han,[†,‡,§] Zuchong Yang,[†,§] Zongkang Li,[†] Xinming Zhuang,[†] Deji Akinwande,[*,‡] and Junsheng Yu[*,†]

[†]State Key Laboratory of Electronic Thin Films and Integrated Devices, School of Optoelectronic Science and Engineering, University of Electronic Science and Technology of China (UESTC), Chengdu 610054, P. R. China

[‡]Microelectronics Research Center, The University of Texas at Austin, Austin, 78758 Texas, United States

Supporting Information

ABSTRACT: Over the past decades, organic field-effect transistor (OFET) gas sensors have maintained a rapid development. However, the majority of OFET gas sensors show insufficient detection capability towards oxidizing gases such as nitrogen oxide, compared with the inorganic counterpart. In this paper, a new strategy of OFET nitrogen dioxide (NO_2) gas sensor, consisting of poly(3-hexylthiophene-2,5-diyl) (P3HT) and poly(9-vinylcarbazole) (PVK) blend, is reported. Depending on the gate voltage, this sensor can operate in two modes at room temperature. Of the two modes exposed to NO_2 for 5 min, when the gate voltage is 0 V, the highest NO_2 responsivity of this OFET is >20 000% for 30 ppm (≈700% for 600 ppb) with the 1:1 P3HT/PVK blend, it is ≈40 times greater than that with the pure P3HT. The limit of detection of ≈300 ppb is achieved, and there is still room for improvement. While in the condition of −40 V, the response increases by 15 times than that with the pure P3HT. This is the first attempt to improve the OFET sensing performance using PVK, which usually functions as a hole-transport layer in the light- emitting device. The enhancement of sensing performance is attributed to the aggregation-controlling and hole-transporting/electron-blocking effect of PVK. This work demonstrates that the hole-transport material can be applied to improve the NO_2 sensor with simple solution process, which expands the material choice of OFET gas sensors.

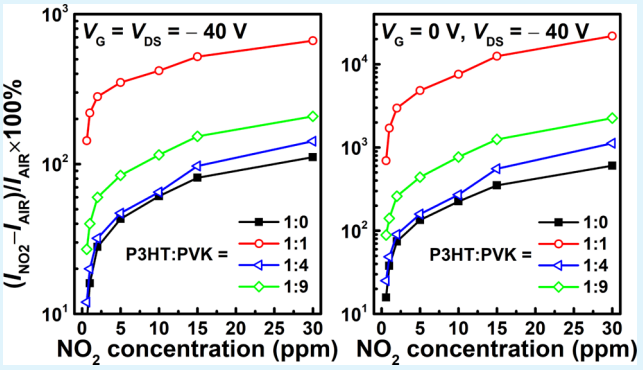

KEYWORDS: *NO_2 gas sensor, polymer blend, organic field-effect transistor (OFET), room temperature, poly(3-hexylthiophene) (P3HT), poly(9-vinylcarbazole) (PVK), gate control*

1. INTRODUCTION

Nitrogen dioxide (NO_2), as one of the main substances of acid rain and photochemical smog, has drawn great attention considering its hazardous effects on humans. However, with the development of modern society, a large amount of NO_2 has been emitted into the environment from vehicles and production processing.[1] Furthermore, NO_2 may cause a serious damage to the human respiration system, even under a low concentration of exposure.[2] Thus, it is urgent to develop a kind of gas sensing device, which can function at room temperature and detect NO_2 at low concentration with high response and excellent performance. Among all kinds of gas sensors, because of their advantages in terms of variety of materials, simple fabrication, low cost, and room- temperature operation, organic semiconductor gas sensors have attracted considerable attention and developed many kinds of gas sensors with different device structures.[3,4] As one kind of them, research on organic field-effect transistor (OFET) gas sensors has been expanding by leaps and bounds over the past decades, because it combines both the signal amplification of a transistor and all the advantages of the organic semiconductor.[5,6] By reasonable optimization, they can detect various kinds of analytes, including gases (such as NH_3 and NO_2), chemicals (such as ethyl acetate, ethylene, and acetone), and bio-molecules.[7−12]

Nearly a dozen years, many works have been done to explore the NO_2 detection application of OFET,[7,8,13,14] but few papers pronounced commensurate response compared to sensors based on metal oxide, carbon nanotubes, and 2D materials.[15−19] By optimization of a pentacene submonolayer, Mirza et al. realized an excellent OFET NO_2 sensor, including high sensitivity, good selectivity, and excellent reproducibility.[20] Another much handy method was developed by Huang et al.[7]

Received: May 12, 2018
Accepted: October 17, 2018
Published: October 17, 2018

DOI: 10.1021/acsami.8b07838
ACS Appl. Mater. Interfaces 2018, 10, 38280−38286

With a simple, low-cost UV−ozone treatment of the gate dielectric surface, the OFET exhibited ultra-high sensitivities and good selectivity. These works represented two main strategies for improving the performance of the OFET gas sensor: Tailoring the organic semiconductor film structure and modulating the semiconductor/dielectric interface.[21,22] Through these strategies, we can optimize the gas adsorption/desorption/diffusion and some other interactions between NO_2 and the semiconductor. As a result, the channel current as one kind of gas response output will be changed significantly.[23]

The mechanism responsible for the channel current change can be attributed to the interaction between the organic semiconductor and NO_2. In terms of p-type OFET, when exposed to NO_2, the hole traps in the channel can be mediated, and additional holes will be released to the channel, thereby the current increases.[24] We can transform the key point of the high response to how to extract the change of holes efficiently. This demands the NO_2 sensitive active layer can have the capacity to accumulate and transport all the indicated holes to the conducting channel. To obtain a high relative response, restraining the effect of electrons should also be considered to improve the signal to noise ratio. However, the electron-blocking/hole-transporting structures have been widely used in the organic photodetectors, organic light-emitting diodes (OLEDs), and organic solar cells (OSCs), it was rarely applied to OFET sensors.[25−27]

In this work, the device structure is essentially the same as that of polymer blend active layer OFET. Poly(3-hexylthiophene-2,5-diyl) (P3HT) and poly(9-vinylcarbazole) (PVK) mixed with different ratios were used to detect NO_2. PVK has a wonderful hole-transporting/electron-blocking capability, as a nonconjugated polymer, it is the first time to be applied to the OFET semiconductor layer to improve the sensing property.[28] The OFETs can operate in two modes depending on the gate voltage (V_G). Their responsivity properties on NO_2 and selectivity to other gases were analyzed. Further, a careful study on the sensing mechanism of the two modes was made considering many factors comprehensively.

2. EXPERIMENTAL DETAILS

2.1. Materials and Polymer Blend Preparation. P3HT (M_w > 45 000, RR = 93%) was purchased from Lumtec Corp., PVK (M_w = 1 100 000) and 1,2-dichlorobenzene (DCB) were both purchased from Sigma-Aldrich. All the above materials were used as received without further purification. P3HT and PVK were dissolved in DCB at the same concentration of 10 mg/mL and vigorously stirred on a magnetic stirring plate overnight. Finally, the two solutions were mixed according to a series of ratios and consecutively stirred for 20 min to ensure sufficient mixing.

2.2. Device Fabrication. As depicted in Figure 1a, the schematic architecture of the gas sensing device is based on a common bottom-gate, top-contact structured OFET with polymer blend as the organic active layer. The OFET was fabricated according to the following process. First, indium tin oxide (ITO) coated glass was used as both substrate and bottom gate electrode. Prior to the deposition of the dielectric layer, the ITO glass substrates were successively cleaned in an ultrasonicated bath with detergent, acetone, deionized water, and isopropanol for 15 min each. These cleaned substrates were dried in an oven at 80 °C for more than 40 min followed by a 10 min ultraviolet−ozone exposure. Second, approximately a 430 nm-thick poly(methyl methacrylate) dielectric layer with a unit capacitance of 5.9 nF/cm^2 was deposited via a two-step spin-coating process which is 500 rpm for 10 s and 1500 rpm for 50 s. Then the dielectric was baked at 90 °C for 2 h to remove the residual solvent. Thirdly, the

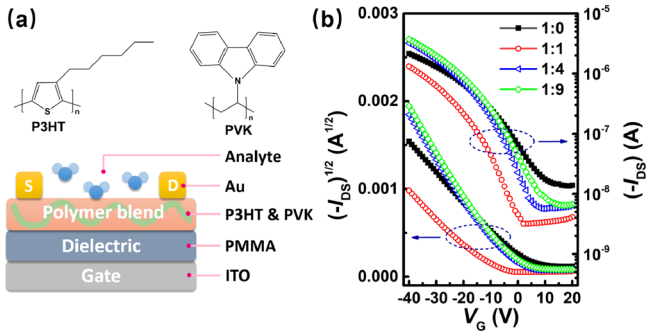

Figure 1. Schematic and electrical characterization of OFET. (a) Chemical structures of P3HT and PVK, a schematic illustration of OFET gas sensor architecture. (b) Transfer curves of OFET with different mix ratios of P3HT and PVK (V_{DS} = −40 V).

well-mixed polymer blend solution was spin-coated utilizing an on-the-fly-dispensing spin-coating approach,[29] wherein the solution was dispensed when the spin-coater motor was already rotating at a fixed rotating speed (here is 2000 rpm). The as-prepared film was immediately annealed on a hot plate at 100 °C for 5 min. Finally, the OFET was completed by depositing the top source and drain electrodes of 40 nm gold via thermal evaporation using a shadow mask at an evaporation rate of 0.5−1 Å/s under 3 × 10^{-3} Pa. The length and width of the active channel were 100 μm and 10 mm, respectively.

2.3. Electrical Measurement and Sensor Evaluation. To evaluate the gas sensing performance, the device was placed into an airtight sensor testing chamber (approximately 2.4 mL). Dry air (background vapor) and certain gas analyte (e.g., 60 ppm standard NO_2) were first mixed at various concentration ratios. Then they were introduced into the test chamber through a mass flow controller. The flow rate was fixed at 100 sccm (standard cm^3 min^{-1}). Along with the ongoing gas flow, transfer and output characteristic curves of the corresponding device at each gas concentration were recorded at intervals of 5 min.

All the electrical characteristics of the OFETs were measured with a Keithley-4200 semiconductor parameter analyzer under ambient conditions. The surface morphology of the active layer was imaged by atomic force microscopy (AFM) (Agilent, AFM 5500) in tapping mode. The inner molecular packing structure was further analyzed by UV−vis spectrophotometer (SHIMADZU UV-1700) measurements.

3. RESULTS AND DISCUSSION

P3HT, a typical conjugated semiconducting polymer, has led to a comprehensive and systematic research on solution-processed OFET. Figure 1b and S1 depict the transfer characteristics of OFETs with different blend ratios of P3HT and PVK. The pure PVK shows no field-effect behavior. The performances of OFETs with other PVK ratios exhibit obvious variation, especially the on/off ratio and I_{DS}. In line with previous reports about the semiconductor/insulator blend system, all the devices with the blend film show a remarkable decrease in off-state current (I_{off}) and subthreshold swing (SS), also increase in field-effect mobility (μ) which is calculated in the saturation regime according to the eq 1

$$I_{DS} = \left(\frac{WC_i}{2L}\right)\mu(V_G - V_{th})^2 \quad (1)$$

where I_{DS} is the drain−source current, L and W are channel length and width, respectively. C_i is the capacitance per unit area of the dielectric layer, V_G is the gate voltage, V_{th} is the threshold gate voltage. The saturated current (I_{DS}, drain current measured at V_{DS} = V_G = −40 V) of the device with

DOI: 10.1021/acsami.8b07838
ACS Appl. Mater. Interfaces 2018, 10, 38280−38286

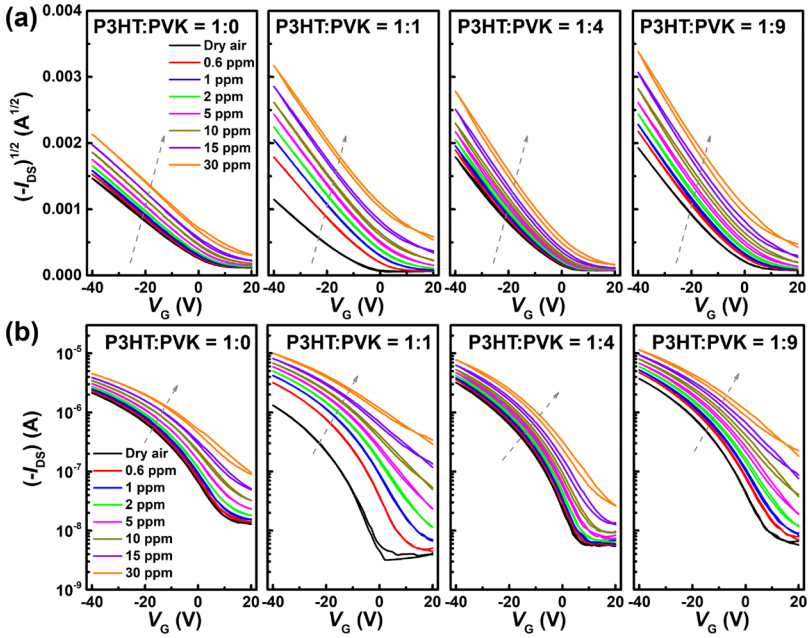

Figure 2. Transfer curves for the indicated P3HT/PVK ratios and different NO_2 concentrations at room temperature (V_{DS} = −40 V). (a) Square root drain−source current vs gate voltage plots. (b) Log plots of drain−source current vs gate voltage.

pure P3HT (2.1 μA) first decreases to ≈1.3 μA for P3HT/PVK = 1:1, next increases to ≈3.2 and ≈3.7 μA as the ratio of PVK is increased from 1:4 to 1:9, respectively. However, due to the decrease of the I_{off}, the on/off ratio increases with the increased ratio of PVK, and then the μ rises from ≈3.61 × 10^{-3} to ≈9.69 × 10^{-3} cm^2 V^{-1} s^{-1} (P3HT/PVK = 1:9).

To evaluate the gas sensing performance of these OFETs with different blend ratios, they were exposed to NO_2 for 5 min in a series of concentrations ranging from 0.6 to 30 ppm with dry air as the background atmosphere to simulate the real sensing scenario. Representative transfer curves recorded at each exposed concentration were measured at V_{DS} of −40 V. As shown in Figure 2, it is obvious that after being blended with PVK, the NO_2 gas sensing ability is not disrupted. On the contrary, all the devices with the blending film show different degrees of enhancement in response to various NO_2 concentrations, the maximum growth comes up in the device with 1:1 blend.

Figure 3 depicts the quantitative changes of key parameters including I_{DS} and μ, when the OFETs interact with various NO_2 concentrations, respectively. The *Y*-axis represents a percentage change defined as $(Y_{NO_2} - Y_{AIR})/Y_{AIR} \times 100\%$. Overall, it can be observed that at all testing concentrations, polymer blend films indeed improve the NO_2 sensing ability of OFETs. For instance, upon exposure to 30 ppm NO_2, the control device with pure P3HT changes its parameters in 111% of I_{DS} and 10% of μ, whereas for the device with 1:1 blend significantly changes in 667% of I_{DS} and 121% of μ. The gas response enhances by a factor of 6 for I_{DS} and 12 for μ. For low concentration, upon exposure to 0.6 ppm NO_2, the change of I_{DS} even further enhances, it increases by 15 times than that of the control device. With a further dilution of P3HT, the responses show an obvious decrease but still compare favorably with those of control device.

Moreover, next to the great benefit to NO_2 sensing improvement, another exceptional advantage of blending PVK with P3HT is a remarkable reduction of the material

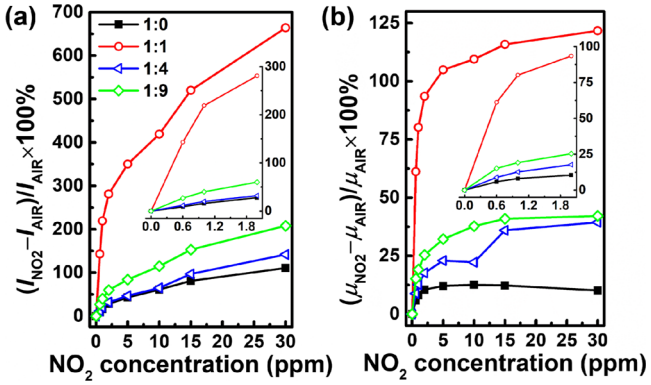

Figure 3. Variation of OFET parameters of indicated P3HT/PVK ratios at different NO_2 concentrations (0.6−30 ppm). (a) Drain−source current. (b) Field-effect mobility (V_G = V_{DS} = −40 V).

cost. The price of commercial high-performance P3HT is >US $ 400 g^{-1}, whereas the cost of PVK is only US$ 10 g^{-1}. When the P3HT is diluted to 10% (1:9), the responses are still more than 3 folds higher than those of the control device, but the price spent per gram of the active material is 8× reduced. Taking the room- temperature detection and solution processing into account, by blending with PVK, indeed we get high performance and low-cost OFET NO_2 sensors.

To reveal the origin of the sensing performance enhancement, the surface topography of the pure P3HT film and the other three blend films were probed by AFM, respectively. As shown in Figure 4, the surface roughness of the blend films is much larger than the pure one. Meanwhile, the mesoscopic phase separation distinctly occurs in the blend films and manifests itself in the protruded structure coexisting with another surrounding matrix. It is a direct consequence of the interplay between liquid−liquid mix and stratification during the spin-coating process.[30,31] In particular, the 1:1 blend film composes of domains (0.5−1 μm in diameter) randomly interspersed in the matrix. On the basis of the developed

DOI: 10.1021/acsami.8b07838
ACS Appl. Mater. Interfaces 2018, 10, 38280−38286

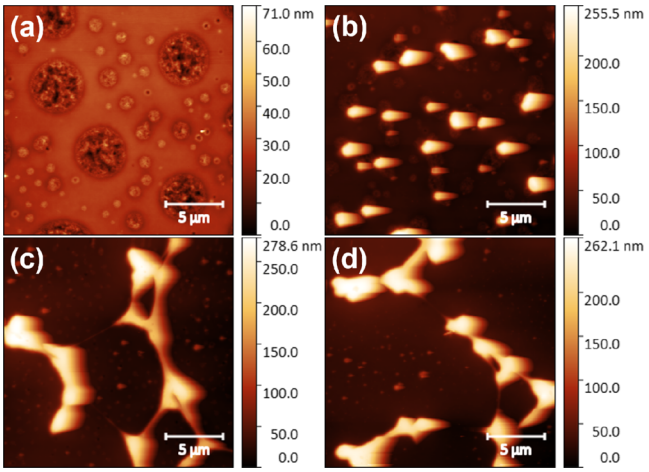

Figure 4. AFM height images (20 μm × 20 μm) of the blend films with different P3HT/PVK ratios. (a) 1:0. (b) 1:1. (c) 1:4. (d) 1:9.

dynamic analyzation of the phase separation process,[32−34] it can be deduced that the raised phase possesses P3HT as the majority component, whereas the surrounding matrix almost entirely consists of PVK.

To acquire a further understanding of the inner thin film structure, UV−vis absorption spectra were measured and demonstrated in Figure 5. Qualitatively, the absorbance peaks

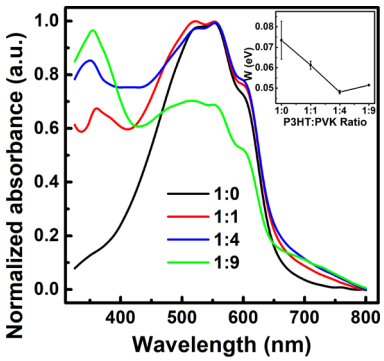

Figure 5. Normalized UV−vis absorption and the free exciton bandwidth of the films with different P3HT/PVK blend ratios.

of P3HT and PVK can be easily identified and the peak height variations reflect the changes of the blend ratio. Further, according to the model of weakly interacting H-aggregate proposed by Spano and Silva,[35] the spectral properties depend on the intermolecular electronic coupling. From the spectra, the free exciton bandwidth (W) of aggregates that is closely related to intrachain order can be extracted using eq 2

$$\frac{I_{0-0}}{I_{0-1}} \approx \left(\frac{1 - 0.24W/E_P}{1 + 0.073W/E_P}\right)^2 \quad (2)$$

where E_P is the main intramolecular vibration energy (0.18 eV), I_{0-0} and I_{0-1} represents the intensity of the (0−0) and (0−1) transition, respectively. Accordingly, for an individual polymer chain, a reduction of W discloses the increase of intramolecular ordering and conjugation in the aggregates. The average value of W for the pure P3HT films appears at 73 meV, whereas in blend films, W has an approximately decreasing trend from 1:1 to 1:4 blends, then slightly increasing for 1:9 blend (52 meV for 1:9 sample) (inset of Figure 5). It indicates that the P3HT becomes planar in the blend film, and the effective conjugation length for charge conducting increases.[36] As a result, the devices with 1:4 and 1:9 blend film show remarkable improvements in the OFET device performance, such as μ and I_{DS}. In addition, the UV−vis absorption results are similar to that got from polystyrene diluted P3HT,[37] but a distinguishable phenomenon in NO_2 sensing. After being blended with PVK, the response is significantly improved, but not increased along with the PVK percentage in the blend film. Hence, we can assume that PVK in the blend film not only functions as an insulating polymer to open the P3HT aggregates but also yields a special contribution to the NO_2 detection.

NO_2 is a strong oxidizing gas which can donate holes to deep trap states or passivate the charge traps of the organic semiconductor, eventually leads to the increase of charge carrier density, which exhibits as the increase in I_{DS} and μ. So how to extract the additional charges and output them as I_{DS} is a key point to the enhancement of response. For the blend with an equal ratio of P3HT/PVK, the effective conjugation length is much disordered than those of 1:4 and 1:9 blend film. The P3HT still partly aggregates in the PVK complex, which results in large energetic disorder and limits the charge conducting.[32] Thus, it shows the lowest saturated I_{DS}. Because PVK always used to improve the hole injection and transport in OLEDs and OSCs, when exposed to NO_2, the additional charges in every individual P3HT chains are extracted by PVK and transport to another P3HT chain. Because of the relatively poor hole mobility of PVK, it can only promote the charge transport of adjacent P3HT chains and cannot function as a conducting material. Therefore, a higher ratio of P3HT is critical to confirm a sufficient distribution in the blend film. For the 1:9 blend, only 10% P3HT remain, but the conjugation length for charge conducting increases, along with an improved mobility. This phenomenon means that P3HT amassed along the conducting channel does not spread randomly in this film, there is less interface to absorb NO_2. However, due to high mobility, the device can still get a good response.

On the basis of the above discussion, the P3HT chains distribute in the blend film and PVK fills the gap between them. It seems that more P3HT and PVK participate in the sensing process, the higher response we can obtain. However, under a bias of gate voltage, the charge transport is limited near to the dielectric/semiconductor interface. Moreover, according to multiple trap and release model,[38] the relationship between effective mobility, free charge density, and trap density can be described as eq 3

$$\mu_{eff} \approx \mu_0 \frac{N_{free}}{N_{free} + N_{trap}} \quad (3)$$

where μ_{eff} is the effective mobility in the channel, μ_0 is the intrinsic mobility of the channel material, N_{free} is the free charge density in the channel and N_{trap} is the trap density. The N_{free} will enlarge exponentially with the gate voltage increase. Meanwhile, the effect of N_{trap} change, related to the NO_2 adsorption, is limited. On the other hand, with the gate voltage decrease, N_{free} will reduce to the same magnitude order of N_{trap}. It seems that a higher response can be obtained under lower gate voltage.

As shown in Figure 2b, OFET with the 1:1 blend film presents an outstanding response at a low gate voltage. Hence, we compared the output curves of control devices to those

DOI: 10.1021/acsami.8b07838
ACS Appl. Mater. Interfaces 2018, 10, 38280−38286

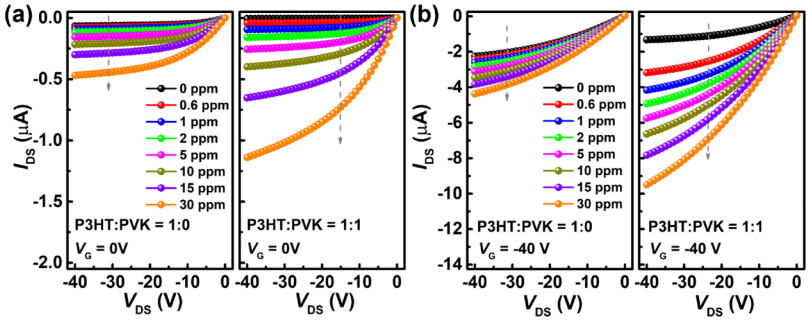

Figure 6. Output curves for the indicated P3HT/PVK ratios under different gate voltages and NO_2 concentrations at room temperature. (a) V_G = −40 V, (b) V_G = 0 V.

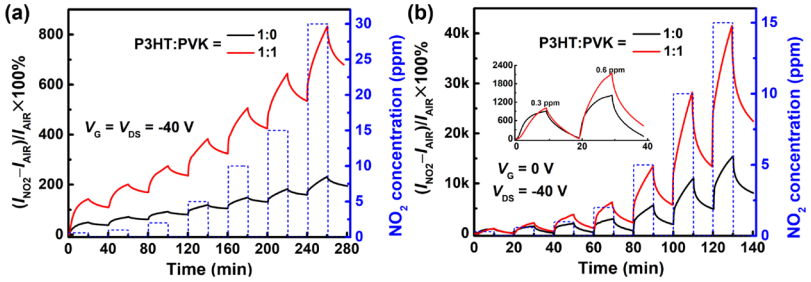

Figure 7. Percentage change of drain current to dynamic NO_2 concentrations at room temperature. (a) $V_G = V_{DS}$ = −40 V. (b) V_G = 0 V, V_{DS} = −40 V.

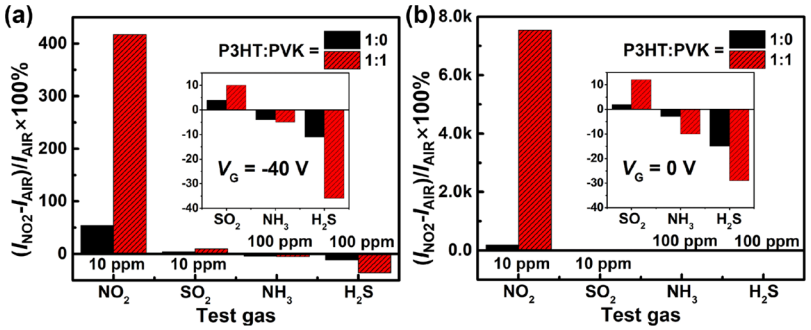

Figure 8. Selectivity test of sensors with pure P3HT and P3HT/PVK = 1:1 for 10 ppm NO_2 and SO_2, and 100 ppm NH_3 and H_2S at room temperature. (a) $V_G = V_{DS}$ = −40 V. (b) V_G = 0 V, V_{DS} = −40 V.

with the 1:1 blend under different NO_2 concentrations at V_G = −40 and 0 V (Figure 6 and Table S1). All the two devices exhibit extraordinary enhancement of detection when the V_G = 0 V, the responsivity at 30 ppm increases from 600% (pure P3HT) to ≈22 000% (1:1), whereas that at 600 ppb increases from 16% to ≈700%. For the individual device under −40 and 0 V gate voltage, the device with 1:1 blend film achieves a five-time enhancement, only two folds got by that with pure P3HT. Moreover, because P3HT can function as an ambipolar active material,[39,40] when V_G = 0 V, with V_{DS} changes from 0 to −40 V, the presence of electron transport should not be ignored in the film because the bias condition favors the accumulation of electrons.[41] PVK, a wide-bandgap polymer, is usually used as a hole-transport material. On the other hand, the PVK restrains the electron transport at 0 V gate voltage. That is why the original current of the device with the 1:1 blend film is much lower than that of pure P3HT. Like the modulation of dark current in the photodetector,[42,43] a lower original current of sensor always denotes a higher response to the same concentration of gases. This result matches the above hypothesis and expands a new kind of operating mode, especially for the subppm NO_2 detection. In addition, the percentage drain current changes of devices with different P3HT/PVK ratios to various NO_2 concentrations are shown in Figure S4.

To further analyze the responsivity of OFET sensors to NO_2, the percentage changes of drain current under different concentrations were monitored at different operation mode. As shown in Figure 7a, the left *Y*-axis is equal to $(I_{NO_2} - I_{AIR})/I_{AIR} \times 100\%$. At V_G = −40 V, each NO_2 pulse keeps 20 min, it can be seen that when the last 30 ppm NO_2 pulse comes, the I_{DS} of the device with 1:1 blend yields an increase of 832% whereas that of device A is 231%, with nearly four times larger response presents. As can be seen in Figure 7b, we reduce the lowest detectable NO_2 concentration down to 300 ppb, and much higher response can be realized to 15 ppm even within the half expose time. In addition, the reproducibility of this OFET sensor with three-cycle test to 5 ppm NO_2 were also measured and shown in Figure S5. It can be clearly observed that the reproducibility under high gate voltage is much better than that under 0 V gate voltage. Note that when applied to long

DOI: 10.1021/acsami.8b07838
ACS Appl. Mater. Interfaces 2018, 10, 38280−38286

enough recovery time, the drain current can be closed to the original current. Moreover, for the further practical application, this device operating under the condition with lower V_{DS} can also be probed. As shown in Figure S6, the device with P3HT/PVK = 1:1 can achieve a 2000% drain current change to 15 ppm NO_2, and 200% to 0.3 ppm, respectively (V_{DS} = −5 V, V_G = 0 V). However, the drain current is still too small. When we change the gate voltage to −5 V, the drain current can be improved slightly, but the drain current change exhibits an obvious decrease.

Because of the limitation of the mass flow controller and gas sources, 0.3 ppm is the lowest concentration of NO_2 that can be reliably utilized in this work. However, the estimated limit of detection (LOD) can be calculated using linear fitting methods.[44,45] Response of I_D versus NO_2 concentration extracted from Figure 7b (P3HT/PVK = 1:1) and the linear fit results are summarized in Figure S7. It has a LOD of 139.3 ppb and a sensitivity of 3448.1% for the low NO_2 concentration detection.

For practical applications, selectivity is another critical parameter, so we investigate the gas selectivity (NO_2 (10 ppm), SO_2 (10 ppm), NH_3 (100 ppm), and H_2S (100 ppm)) at two different modes, and the results are shown in Figure 8. It is obvious that for the OFET with the 1:1 blend film, all of the other gases are at least 9× less than the NO_2 (Figure 8a). For V_G = 0 V, the responsivity of the OFET with the 1:1 film is so large that the response of other gases cannot be displayed (Figure 8b). For clarity, a separate plot with much smaller *Y*-axis is illuminated (inset of Figure 8b). It can be seen that this platform can clearly distinguish NO_2 from SO_2, which is another major poisonous gas in air. The lone electron in NO_2 also means that this compound is a free radical, which renders NO_2 highly chemically reactive compared with SO_2. As the p-doping of conducting polymer can be accomplished by electrochemically or chemically oxidation, the p-doping effect of NO_2 is much more efficient than that of SO_2. When the gate bias reduced to 0 V, the holes in the conducting channel accumulated by the negative gate bias dropped dramatically, the drain current is dependent on the intrinsic conductivity of P3HT accordingly. As a result, the doping effect is the main sensing mechanism, that's why the selectivity at lower V_G is further improved. And the reducing gases, which has opposite change compared with the oxidizing gas of NO_2, cause little impact to NO_2 detection.

Combining with the above results obtained from the output curves under various NO_2 concentrations, we can see that the obtained gas sensors can work with two different modes. When the sensor works at V_G = −40 V, with a high signal−noise ratio, it can be used for long-term real-time and quantitative gas detection. If we just need a qualitative monitoring of NO_2 in a certain area, the mode working at 0 V could be a better choice for low- power and fast detection.

4. CONCLUSIONS

In this work, a novel strategy of ultrahigh responsivity and sensitivity, good selectivity, and low-cost OFET-based NO_2 sensors has been realized with P3HT/PVK blend active layer. PVK can not only increase the adsorption interface of P3HT but also extract the additional hole released by traps. The highest NO_2 responsivity of these OFETs is >20 000% for 30 ppm (≈700% for 600 ppb) with the 1:1 P3HT/PVK blend, which ≈40 times higher than that with the pure P3HT. The LOD of ≈300 ppb is achieved, and by using the linear fitting calculation it can yield a LOD of 139.3 ppb. In the case of practical application area, two operating modes are available. Thus, we believe that this strategy, together with the advantages of low material cost, simple OFET fabrication, and multiple operating modes, opens up an effective method to achieve the high performance gas sensors.

■ ASSOCIATED CONTENT

Supporting Information

The Supporting Information is available free of charge on the ACS Publications website at DOI: 10.1021/acsami.8b07838.

Electrical properties of pure PVK films, more AFM images, and OFET characterization related to the low voltage, repeatability and LOD calculation (PDF)

■ AUTHOR INFORMATION

Corresponding Authors

*E-mail: deji@ece.utexas.edu (D.A.).
*E-mail: jsyu@uestc.edu.cn (J.Y.).

ORCID

Junsheng Yu: 0000-0002-7484-8114

Author Contributions

§S.H. and Z.Y. contributed equally to this work.

Notes

The authors declare no competing financial interest.

■ ACKNOWLEDGMENTS

This work was financially supported by the Foundation of Innovation Research Groups of the National Natural Science Foundation of China (NSFC) (grant no. 61421002), the Foundation for National Key R&D Program of China (grant no. 2018YFB0407100-02), the Foundation of NSFC (grant nos. 61675041 & 51703019), State Scholarship Fund of China Scholarship Council (grant no. 201606070044). We also thank Xiao Wang of Microelectronics Research Center of UT Austin for helpful discussions of the sensing mechanism.

■ REFERENCES

(1) AGENCY, E. P. *Review of the Primary National Ambient Air Quality Standards for Oxides of Nitrogen Federal Register*, 2018, 83.

(2) Hamra, G. B.; Laden, F.; Cohen, A. J.; Raaschou-Nielsen, O.; Brauer, M.; Loomis, D. Lung Cancer and Exposure to Nitrogen Dioxide and Traffic: A Systematic Review and Meta-Analysis. *Environ. Health Perspect.* **2015**, *123*, 1107−1112.

(3) Wang, Z.; Huang, L.; Zhu, X.; Zhou, X.; Chi, L. An Ultrasensitive Organic Semiconductor NO_2 Sensor Based on Crystalline TIPS-Pentacene Films. *Adv. Mater.* **2017**, *29*, 1703192.

(4) Huang, L.; Wang, Z.; Zhu, X.; Chi, L. Electrical Gas Sensors Based on Structured Organic Ultra-Thin Films and Nanocrystals on Solid State Substrates. *Nanoscale Horiz.* **2016**, *1*, 383−393.

(5) Zhang, C.; Chen, P.; Hu, W. Organic Field-Effect Transistor-Based Gas Sensors. *Chem. Soc. Rev.* **2015**, *44*, 2087−2107.

(6) Guo, Y.; Yu, G.; Liu, Y. Functional Organic Field-Effect Transistors. *Adv. Mater.* **2010**, *22*, 4427−4447.

(7) Huang, W.; Zhuang, X.; Melkonyan, F. S.; Wang, B.; Zeng, L.; Wang, G.; Han, S.; Bedzyk, M. J.; Yu, J.; Marks, T. J.; Facchetti, A. UV-Ozone Interfacial Modification in Organic Transistors for High-Sensitivity NO_2 Detection. *Adv. Mater.* **2017**, *29*, 1701706.

(8) Shi, W.; Yu, J.; Katz, H. E. Sensitive and Selective Pentacene-Guanine Field-Effect Transistor Sensing of Nitrogen Dioxide and Interferent Vapor Analytes. *Sens. Actuators, B* **2018**, *254*, 940−948.

DOI: 10.1021/acsami.8b07838
ACS Appl. Mater. Interfaces 2018, 10, 38280−38286

(9) Huang, W.; Yu, J.; Yu, X.; Shi, W. Polymer Dielectric Layer Functionality in Organic Field-Effect Transistor Based Ammonia Gas Sensor. *Org. Electron.* **2013**, *14*, 3453−3459.
(10) Han, S.; Zhuang, X.; Jiang, Y.; Yang, X.; Li, L.; Yu, J. Poly(vinyl alcohol) as a Gas Accumulation Layer For An Organic Field-Effect Transistor Ammonia Sensor. *Sens. Actuators, B* **2017**, *243*, 1248−1254.
(11) Torsi, L.; Magliulo, M.; Manoli, K.; Palazzo, G. Organic Field-Effect Transistor Sensors: A Tutorial Review. *Chem. Soc. Rev.* **2013**, *42*, 8612−8628.
(12) Besar, K.; Dailey, J.; Katz, H. E. Ethylene Detection Based on Organic Field-Effect Transistors With Porogen and Palladium Particle Receptor Enhancements. *ACS Appl. Mater. Interfaces* **2017**, *9*, 1173−1177.
(13) Zhuang, X.; Huang, W.; Han, S.; Jiang, Y.; Zheng, H.; Yu, J. Interfacial Modifying Layer-Driven High-Performance Organic Thin-Film Transistors and Their Nitrogen Dioxide Gas Sensors. *Org. Electron.* **2017**, *49*, 334−339.
(14) Fan, H.; Shi, W.; Yu, X.; Yu, J. High Performance Nitrogen Dioxide Sensor Based on Organic Field-Effect Transistor Utilizing Ultrathin CuPc/PTCDI-C8 Heterojunction. *Synth. Met.* **2016**, *211*, 161−166.
(15) Afzal, A.; Cioffi, N.; Sabbatini, L.; Torsi, L. NO_x Sensors Based on Semiconducting Metal Oxide Nanostructures: Progress and Perspectives. *Sens. Actuators, B* **2012**, *171-172*, 25−42.
(16) Wang, X.; Su, J.; Chen, H.; Li, G.; Shi, Z.; Zou, H.; Zou, X. Ultrathin In_2O_3 Nanosheets with Uniform Mesopores for Highly Sensitive Nitric Oxide Detection. *ACS Appl. Mater. Interfaces* **2017**, *9*, 16335−16342.
(17) Singh, E.; Meyyappan, M.; Nalwa, H. S. Flexible Graphene-Based Wearable Gas and Chemical Sensors. *ACS Appl. Mater. Interfaces* **2017**, *9*, 34544−34586.
(18) Zhang, M.; Su, H. C.; Rheem, Y.; Hangarter, C. M.; Myung, N. V. A Rapid Room-Temperature NO_2 Sensor Based on Tellurium-SWNT Hybrid Nanostructures. *J. Phys. Chem. C* **2012**, *116*, 20067−20074.
(19) Cui, S.; Pu, H.; Wells, S. A.; Wen, Z.; Mao, S.; Chang, J.; Hersam, M. C.; Chen, J. Ultrahigh Sensitivity and Layer-Dependent Sensing Performance of Phosphorene-Based Gas Sensors. *Nat. Commun.* **2015**, *6*, 8632.
(20) Mirza, M.; Wang, J.; Wang, L.; He, J.; Jiang, C. Response enhancement mechanism of NO_2 gas sensing in ultrathin pentacene field-effect transistors. *Org. Electron.* **2015**, *24*, 96−100.
(21) Zang, Y.; Huang, D.; Di, C.; Zhu, D. Device Engineered Organic Transistors for Flexible Sensing Applications. *Adv. Mater.* **2016**, *28*, 4549−4555.
(22) Wu, X.; Mao, S.; Chen, J.; Huang, J. Strategies for Improving the Performance of Sensors Based on Organic Field-Effect Transistors. *Adv. Mater.* **2018**, *30*, 1705642.
(23) Duarte, D.; Dodabalapur, A. Investigation of The Physics of Sensing in Organic Field Effect Transistor Based Sensors. *J. Appl. Phys.* **2012**, *111*, 044509.
(24) Andringa, A.-M.; Piliego, C.; Katsouras, I.; Blom, P. W. M.; Leeuw, D. M. NO_2 Detection and Real-Time Sensing with Field-Effect Transistors. *Chem. Mater.* **2014**, *26*, 773−785.
(25) Caranzi, L.; Pace, G.; Sassi, M.; Beverina, L.; Caironi, M. Transparent and Highly Responsive Phototransistors Based on a Solution-Processed, Nanometers-Thick Active Layer, Embedding a High-Mobility Electron-Transporting Polymer and a Hole-Trapping Molecule. *ACS Appl. Mater. Interfaces* **2017**, *9*, 28785−28794.
(26) Luber, E. J.; Buriak, J. M. Reporting Performance in Organic Photovoltaic Devices. *ACS Nano* **2013**, *7*, 4708−4714.
(27) Bell, B. M.; Clark, M. B.; Devore, D. D.; De Vries, T. S.; Froese, R. D.; Gray, K. C.; Jackson, D. H. K.; Kuech, T. F.; Na, H.-Y.; Kearns, K. L.; Lee, K.-J.; Mukhopadhyay, S.; Rachford, A. A.; Spencer, L. P.; Woodward, W. H. H. Degradation of Hole Transport Materials via Exciton-Driven Cyclization. *ACS Appl. Mater. Interfaces* **2017**, *9*, 13369−13379.
(28) Tao, Y.; Yang, C.; Qin, J. Organic Host Materials for Phosphorescent Organic Light-Emitting Diodes. *Chem. Soc. Rev.* **2011**, *40*, 2943−2970.
(29) Zhang, F.; Di, C.; Berdunov, N.; Hu, Y.; Gao, X.; Meng, Q.; Sirringhaus, H.; Zhu, D.; Zhu, D. Ultrathin Film Organic Transistors: Precise Control of Semiconductor Thickness via Spin-Coating. *Adv. Mater.* **2013**, *25*, 1401−1407.
(30) Kim, M.; Lee, J.; Jo, S. B.; Sin, D. H.; Ko, H.; Lee, H.; Lee, S. G.; Cho, K. Critical Factors Governing Vertical Phase Separation in Polymer-Pcbm Blend Films for Organic Solar Cells. *J. Mater. Chem. A* **2016**, *4*, 15522−15535.
(31) Kim, J.-S.; Ho, P. K. H.; Murphy, C. E.; Friend, R. H. Phase Separation in Polyfluorene-Based Conjugated Polymer Blends: Lateral and Vertical Analysis of Blend Spin-Cast Thin Films. *Macromolecules* **2004**, *37*, 2861−2871.
(32) Abbaszadeh, D.; Kunz, A.; Wetzelaer, G. A. H.; Michels, J. J.; Crăciun, N. I.; Koynov, K.; Lieberwirth, I.; Blom, P. W. M. Elimination of Charge Carrier Trapping in Diluted Semiconductors. *Nat. Mater.* **2016**, *15*, 628−633.
(33) Coveney, S.; Clarke, N. Pattern Formation in Polymer Blend Thin Films: Surface Roughening Couples to Phase Separation. *Phys. Rev. Lett.* **2014**, *113*, 218301.
(34) Yim, K.-H.; Doherty, W. J.; Salaneck, W. R.; Murphy, C. E.; Friend, R. H.; Kim, J.-S. Phase-Separated Thin Film Structures for Efficient Polymer Blend Light-Emitting Diodes. *Nano Lett.* **2010**, *10*, 385−392.
(35) Spano, F. C.; Silva, C. H- and J-Aggregate Behavior in Polymeric Semiconductors. *Annu. Rev. Phys. Chem.* **2014**, *65*, 477−500.
(36) Wang, G.; Persson, N.; Chu, P.-H.; Kleinhenz, N.; Fu, B.; Chang, M.; Deb, N.; Mao, Y.; Wang, H.; Grover, M. A.; Reichmanis, E. Microfluidic Crystal Engineering of π-Conjugated Polymers. *ACS Nano* **2015**, *9*, 8220−8230.
(37) Han, S.; Zhuang, X.; Shi, W.; Yang, X.; Li, L.; Yu, J. Poly(3-hexylthiophene)/Polystyrene (P3HT/PS) Blends Based Organic Field-Effect Transistor Ammonia Gas Sensor. *Sens. Actuators, B* **2016**, *225*, 10−15.
(38) Li, L.; Lu, N.; Liu, M. Field Effect Mobility Model in Oxide Semiconductor Thin Film Transistors With Arbitrary Energy Distribution of Traps. *IEEE Electron Device Lett.* **2014**, *35*, 226−228.
(39) Choulis, S. A.; Kim, Y.; Nelson, J.; Bradley, D. D. C.; Giles, M.; Shkunov, M.; McCulloch, I. High Ambipolar and Balanced Carrier Mobility in Regioregular Poly(3-Hexylthiophene). *Appl. Phys. Lett.* **2004**, *85*, 3890−3892.
(40) Zaumseil, J.; Sirringhaus, H. Electron and Ambipolar Transport in Organic Field-Effect Transistors. *Chem. Rev.* **2007**, *107*, 1296−1323.
(41) Dutta, S.; Lewis, S. D.; Dodabalapur, A. Hybrid Organic/Inorganic Ambipolar Thin Film Transistor Chemical Sensor. *Appl. Phys. Lett.* **2011**, *98*, 213504.
(42) Wang, X.; Huang, J.; Han, S.; Yu, J. High Photoresponse Inverted Ultraviolet Photodectectors Consisting of Iridium Phosphor Doped into Poly(N-Vinylcarbazole) Polymeric Matrix. *Appl. Phys. Lett.* **2014**, *104*, 173304.
(43) Guo, F.; Yang, B.; Yuan, Y.; Xiao, Z.; Dong, Q.; Bi, Y.; Huang, J. A Nanocomposite Ultraviolet Photodetector Based on Interfacial Trap-Controlled Charge Injection. *Nat. Nanotechnol.* **2012**, *7*, 798−802.
(44) Li, J.; Lu, Y.; Ye, Q.; Cinke, M.; Han, J.; Meyyappan, M. Carbon Nanotube Sensors for Gas and Organic Vapor Detection. *Nano Lett.* **2003**, *3*, 929−933.
(45) Zheng, H.; Ramalingam, B.; Korampally, V.; Gangopadhyay, S. Large Sensitivity Enhancement in Semiconducting Organic Field Effect Transistor Sensors Through Incorporation of Ultra-Fine Platinum Nanoparticles. *Appl. Phys. Lett.* **2013**, *103*, 193305.

DOI: 10.1021/acsami.8b07838
ACS Appl. Mater. Interfaces 2018, 10, 38280−38286